Understanding Creep—a Review

W. BLUM, P. EISENLOHR, and F. BREUTINGER

A simple model based on the Orowan equation and the dynamic evolution of the dislocation structure by generation and merging of slipped areas is used to see which experimental results on creep of pure and solute-hardened crystalline materials can or cannot be explained with regard to creep with refinement or coarsening of the dislocation structure and steady-state creep. Quantitative deficiencies of the model for pure materials are discussed; most of them are related to neglection of subgrain formation.

I. INTRODUCTION

A. *Experimental Basis*

CREEP of materials is time-dependent inelastic deformation at constant stress, σ. A creep test begins with loading of the specimen. The loading procedure is usually ill-defined. For simplicity, it is assumed in Figure 1 that the total strain rate, $\dot{\varepsilon}_{\text{tot}}$, has a constant high value in the loading phase. The total strain, ε_{tot}, is the sum of the elastic strain $\varepsilon_{el} = \sigma/E$ (for uniaxial loading, E: Young's modulus) and the inelastic strain, $\varepsilon_{\text{inel}}$, which is itself additively composed from the anelastic (time-dependent reversible) and the plastic (time-dependent irreversible) strains, $\varepsilon_{\text{anel}}$ and ε_{pl}:

$$\varepsilon_{\text{tot}} = \varepsilon_{el} + \varepsilon_{\text{inel}} = \sigma/E + \varepsilon_{\text{inel}} \quad \varepsilon_{\text{inel}} = \varepsilon_{\text{anel}} + \varepsilon_{pl} \qquad [1]$$

The values of ε_{el} and $\varepsilon_{\text{anel}}$ increase as σ increases during loading. When loading is complete, the elastic strain rate drops to zero. Similarly, the anelastic strain rate disappears within a relatively small strain interval where the anelastic strain saturates. Subsequently, the total strain rate, $\dot{\varepsilon}_{\text{tot}}$, during creep (at constant stress) equals the plastic strain rate, $\dot{\varepsilon}_{pl}$.*

*In the following, we will drop the subscript *pl* unless differentiation between $\dot{\varepsilon}_{\text{tot}}$ and $\dot{\varepsilon}_{pl}$ is required.

As $\dot{\varepsilon}_{pl}$ depends on σ and is independent of $\dot{\sigma}$, the rate of plastic straining, $\dot{\varepsilon}_{pl}$, at the beginning of creep is identical to the rate of creep at the end of loading. This means that there must be plastic straining during loading for creep to occur; in other words, the loading strain prior to creep necessarily contains a plastic component. This holds even if creep is investigated at stresses below the *yield stress* (defining the stress for the onset of plastic straining at a fixed, *high* rate of straining, *e.g.*, $\dot{\varepsilon}_{\text{tot}} = 10^{-4}$/s).

The presentation of creep as $\dot{\varepsilon}_{\text{tot}}$ *vs* ε_{tot}, as in Figure 1, is most convenient for showing the whole deformation history. In many applications, however, it is preferred to show the progress of strain, ε, with time, t.* The obvious disadvantage of this traditional way of presenting creep is that each creep curve has a different shape in the ε-t plot. With the average creep rate varying over many orders of magnitude, the ε-t curves vary from nearly vertical to nearly horizontal. A nearly horizontal ε-t curve gives the impression of steady-state deformation even though the limitation in ε excludes such statement. Many statements on seemingly minimum or steady-state rates are unfounded due to inappropriate limitation of the investigated strain interval.

*The exact meaning of ε is often unclear. Clear distinction between the different strain terms is most important for interpretation of results in the range of low creep rates where ε_{tot} is small.

The problem of displaying the ε-t data has the rather absurd consequence that creep data are frequently condensed to what is called *the creep rate*, addressing the minimum or steady-state creep rate. Thus, in a significant fraction of publications on creep, it is impossible to check the data base for relevance. This is in contrast to research on work hardening where the data base is formed by the σ-ε curves and weakens the scientific basis of creep research, leaving the reader only the chance of either believing the published $\dot{\varepsilon}$ data or repeating the experiments. Often both alternatives are unacceptable. Publishing the log $\dot{\varepsilon}$-ε curves is a convenient way of avoiding the problem.*

*The scatter resulting from the differentiation procedure is not a real problem because it can easily be limited by choosing sufficiently large strain intervals $\Delta\varepsilon$, *e.g.*, 10^{-3}, for determining the local creep rate $\dot{\varepsilon} = \Delta\varepsilon/\Delta t$.

B. *Theoretical Framework*

Crystalline materials deform plastically by dislocation motion. This holds also for creep (as defined in the preceding), regardless of the fact that complementary mechanisms of plastic deformation, such as sliding of grain boundaries and diffusive flow, exist. However, in most cases, generation, motion, and annihilation of dislocations are indispensable for carrying creep on to strains in the order of 10^{-2}. The dislocation activity becomes apparent through the formation of characteristic cellular or subgranular patterns where dislocations arrange in walls at the boundaries of cells/subgrains with relatively low internal dislocation density. Only in rare cases do such patterns not evolve during continued uniaxial deformation. One example is deformation of materials that are so fine-grained that the specific large angle grain-boundary area is sufficient to absorb the dislocations being generated during flow, before they have the chance to form cells, and superplastic behavior may result.

W. BLUM, Professor, P. EISENLOHR, Teaching and Research Associate, and F. BREUTINGER, Research Associate, are with the Institut für Werkstoffwissenschaften, University of Erlangen-Nürnberg, 91058 Erlangen, Germany.

This article is based on a presentation made in the workshop entitled "Mechanisms of Elevated Temperature Plasticity and Fracture," which was held June 27–29, 2001, in San Diego, CA, concurrent with the 2001 Joint Applied Mechanics and Materials Summer Conference. The workshop was sponsored by Basic Energy Sciences of the United States Department of Energy.

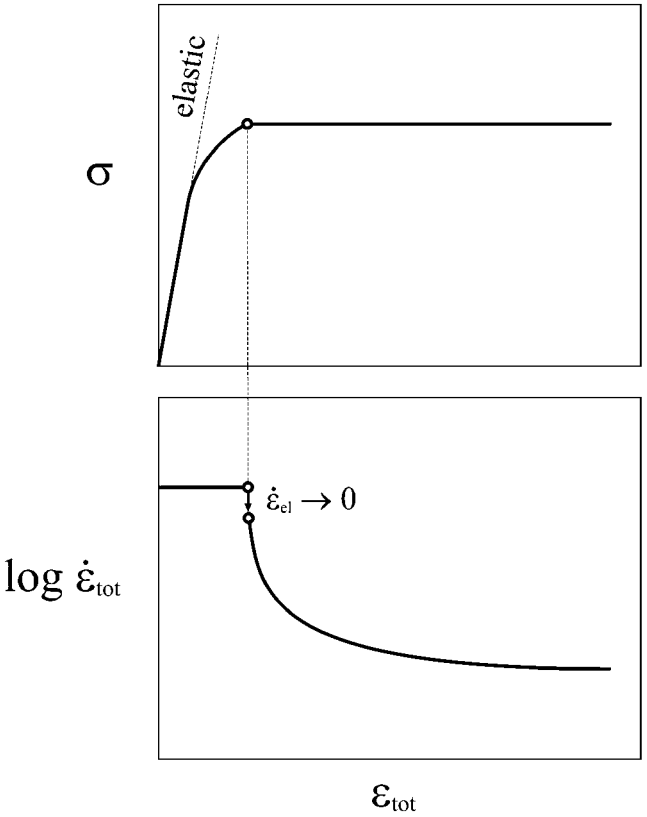

Fig. 1—Variation of stress σ and total strain rate $\dot{\varepsilon}_{tot}$ with total strain ε_{tot} in a creep test. The sudden decrease in $\dot{\varepsilon}_{tot}$ at the end of loading results from $\dot{\varepsilon}_{el}$ falling to 0; its magnitude depends on the magnitude of the ratio $\dot{\varepsilon}_{el}/\dot{\varepsilon}_{tot}$ at the end of loading.

In the last decades, a lot of knowledge on dislocations has been accumulated. This knowledge must enter the constitutive relations governing plastic deformation, also called mechanical equations of state, describing the evolution of the dislocation structure and the kinetics of dislocation motion. In the following, we will collect basic constitutive relations of plasticity in the simplest possible form and use them to check which of the salient features of creep of single-phase materials can be understood without problems and to identify gaps in our understanding.

II. CONSTITUTIVE RELATIONS

The rate of creep, $\dot{\varepsilon}$, is proportional to the area slipped per unit time and volume, given as the product of density, ρ_{mob}, and average glide velocity, v_g, of mobile dislocations:

$$\dot{\varepsilon} = M^{-1}\, b \rho_{mob}\, v_g \qquad [2]$$

(b: Burgers vector length and M: geometrical factor (for polycrystals: Taylor factor)). This basic law of plasticity (Orowan equation) has been used successfully by many in conjunction with formulae for dislocation structure evolution to explain certain basic features of creep (*e.g.*, References 1 and 2), such as the normal and inverse transients and the steady-state behavior. The weakest point in such descriptions is the phenomenologic nature of dislocation structure evolution. It is well known that dislocation annihilation is equivalent to dipole dissolution (*e.g.*, Weertman[3,4] and Blum[5]). However, the density of dislocations in dipole configuration is rarely introduced explicitly as a microstructural parameter. Exceptions are the works of Nes[6] and Roters *et al.*[7,8]

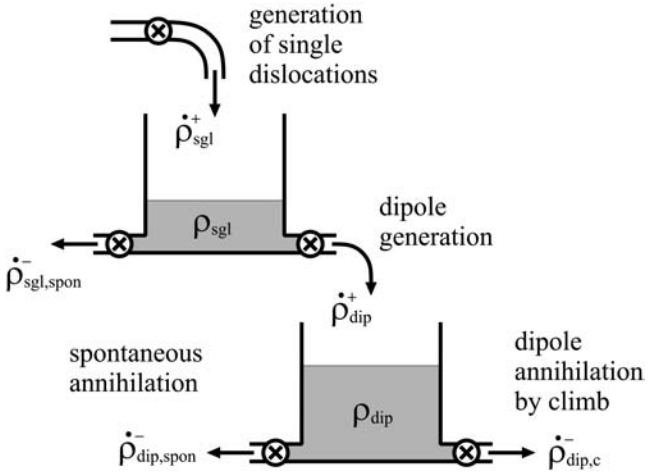

Fig. 2—Scheme of dislocation structure evolution: single dislocations may either annihilate spontaneously or form dipoles. Dipoles disappear either by spontaneous annihilation or by dissolution *via* climb or cross slip.

In the spirit of the latter articles we introduce a simple model containing as essential features

(1) the evolution of the dislocation structure by
   (a) generation of dislocations and
   (b) formation and annihilation of dipoles, and
(2) the kinetics of dislocation motion.

The complication of structural heterogeneity due to formation of cell or subgrain boundaries is deliberately omitted in order to see the merits and shortcomings of the simple approach.

A. *Evolution of Dislocation Structure*

Figure 2 shows the schematic evolution of the dislocation structure for a single Burgers vectors. The real structure evolution results from the superposition of activity of dislocations with different Burger's vectors. Two types of dislocations are discerned, the "singles" and those dislocations that have been captured in a dipolar configuration:

$$\rho = \rho_{sgl} + \rho_{dip} \qquad [3]$$

Each of the two dislocation "containers" for singles and dipoles has two outlets, one representing spontaneous annihilation and the second one formation or annihilation of dipoles. Spontaneous annihilation occurs once the dipole partners come so close to each other that the dislocation line energy is sufficient to produce the lattice defects remaining when the dislocations disappear.[9] The rate equations are

$$\dot{\rho}_{sgl} = \dot{\rho}^{+}_{sgl} - \dot{\rho}^{-}_{sgl} \qquad [4]$$

$$\dot{\rho}^{-}_{sgl} = \dot{\rho}^{+}_{dip} + \dot{\rho}^{-}_{sgl,spon} \qquad [5]$$

$$\dot{\rho}_{dip} = \dot{\rho}^{+}_{dip} - \dot{\rho}^{-}_{dip} \qquad [6]$$

$$\dot{\rho}^{-}_{dip} = \dot{\rho}^{-}_{dip,c} + \dot{\rho}^{-}_{dip,spon} \qquad [7]$$

In the following, the rate terms of the preceding expressions will be quantified.

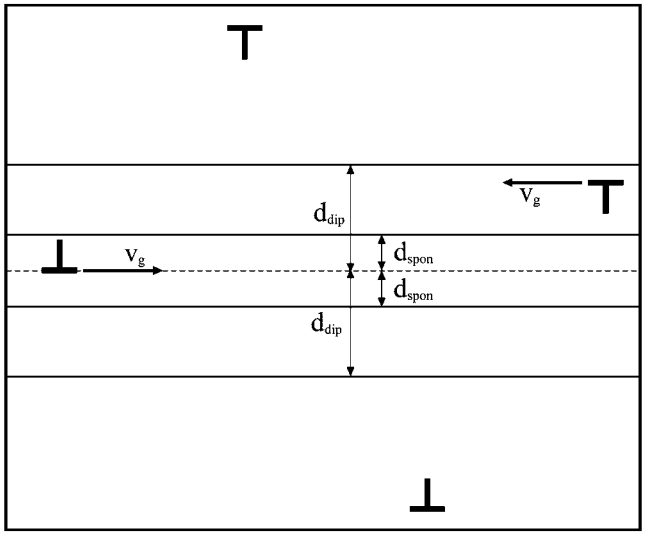

Fig. 3—Capture of single dislocations by dipole formation within a slip plane spacing of d_{dip}. Within the spacing $<d_{spon}$, the dipole disappears spontaneously.[7]

1. *Dislocation generation*

Single dislocations are generated in the course of plastic deformation at the rate:

$$\dot{\rho}^{+}_{sgl} = \frac{M}{b}\frac{\dot{\varepsilon}}{\Lambda^{+}} \qquad [8]$$

By definition of strain, $1/\Lambda^{+}$ is the dislocation length generated per slipped area. In a one-dimensional model with parallel dislocations, Λ^{+} represents the total distance by which a dislocation glides during its life; if dislocations form circular loops expanding up to a maximum radius, r, Λ^{+} equals $r/2$. Following the literature,[6] Λ^{+} is set proportional to the average spacing of dislocations:

$$\Lambda^{+} = k_{\Lambda}\rho^{-0.5} \qquad [9]$$

(k_{Λ}: numerical constant).

2. *Loss of single dislocations*

When a dislocation meets another one of opposite sign lying in a slip plane that is less than a certain distance, d_{dip}, apart, the two dislocations get stuck in a dipolar configuration (Figure 3). The rate at which single dislocations are lost by dipole capture equals the volume fraction, $(M/b)\,\dot{\varepsilon}\,2d_{dip}$, sampled per time for potential reaction partners times twice the length per volume of such partners equaling $2(1/(2n_g))\rho_{sgl}$, where the factor 2 is appropriate, if the reaction partners are themselves moving at the velocity, v_g, into the sampled volume, and n_g is the number of active slip systems so that $1/(2n_g)$ is the average fraction of dislocations with the given Burgers vector, but opposite sign. Thus,

$$\dot{\rho}^{-}_{sgl} = (M/b)\dot{\varepsilon}\,2d_{dip} \times 2 \times \frac{\rho_{sgl}}{n_g} \qquad [10]$$

If the spacing between the slip planes of the dipole partners is smaller than d_{spon}, the dipole disappears spontaneously leaving debris in the form of point defects or their agglomerates behind.[9] Thus,

$$\dot{\rho}^{-}_{sgl,spon} = \frac{d_{spon}}{d_{dip}}\,\dot{\rho}^{-}_{sgl} \qquad [11]$$

The rest remains in dipolar configuration, which means (Eq. [5]) that dipoles with an average slip-plane spacing of $(d_{dip} + d_{spon})/2$ are generated at the rate $\dot{\rho}^{+}_{dip} = \dot{\rho}^{-}_{sgl} - \dot{\rho}^{-}_{sgl,spon}$.

3. *Loss of dislocation dipoles*

For slip-plane spacings between d_{spon} and d_{dip}, the two dipole partners approach each other by climb or cross slip until their spacing has decreased to d_{spon}. The corresponding rate of annihilation is

$$\dot{\rho}^{-}_{dip,c} = \rho_{dip}\nu_{dip} \qquad \nu_{dip} = \frac{2v_c}{(d_{dip} - d_{spon})/2} \qquad [12]$$

ν_{dip} is the frequency at which dipoles of average width dissolve as each of the dipole dislocations moves in the direction perpendicular to the slip plane at the average velocity, v_c. The formation of dipoles and their disappearance through annihilation of the dipole dislocations represent dynamic recovery. The dipole capture spacing depends on stress (passing stress for parallel edge dislocations[10]):

$$d_{dip} = \frac{M}{8\pi(1-\nu)}\frac{Gb}{\sigma} \qquad [13]$$

(G: shear modulus, and ν: Poisson's ratio). In addition to this thermally activated process of loss of dipoles, there is an athermal one in the form of spontaneous annihilation. Dipole dislocations may be annihilated spontaneously by a single dislocation passing by within d_{spon}. The incoming single dislocation and one partner of the dipole annihilate, the remaining partner of the dipole becomes a single. In result, the single dislocation density remains unchanged, and the dipole disappears. Considering reaction partner density, relative velocity of interaction partners, and interaction distance, one obtains in analogy to Eq. [10], noting that dipoles do not move:

$$\dot{\rho}^{-}_{dip,spon} = (M/b)\dot{\varepsilon}\,2d_{spon} \times \frac{\rho_{dip}}{n_g} \qquad [14]$$

B. *Kinetics of Dislocation Motion*

1. *Glide*

The fraction f_{mob} of the single dislocations is assumed to be mobile by glide:

$$\rho_{mob} = f_{mob}\,\rho_{sgl} \qquad [15]$$

The glide velocity, v_g, depends not only on applied stress, σ, at a given temperature, T, but is limited by dislocation interaction. According to the classical effective stress approach, v_g is a monotonically increasing function of the effective stress available for motion:

$$\sigma^{*} = \sigma - \sigma_i \qquad [16]$$

with $v_g = 0$ for $\sigma^{*} = 0$. The athermal stress component, σ_i, depends on the dislocation density as

$$\sigma_i = \alpha MCGb\,\sqrt{\rho_{sgl} + c_{dip}\rho_{dip}} \qquad [17]$$

α is the dislocation interaction constant, the numerical factor C, with $|C| < 1$, relates to anelastic deformation, and c_{dip} is a weighting factor.

a. *Jerky glide*

Thermally activated overcoming of obstacles leads to jerky glide with the velocity:[11]

$$v_g = \lambda_0 \frac{b}{\lambda} \nu_D \exp\left(-\frac{\Delta G_0}{k_B T}\right) 2 \sinh\left(\frac{\Delta W}{k_B T}\right) \quad [18]$$

$$\Delta W = b \Delta a^* \sigma^* / M \qquad \Delta W < \Delta G_0 \quad [19]$$

λ_0 is the mean planar-obstacle spacing, ν_D is the Debye frequency, λ is the spacing of thermal obstacles along the dislocation lines, ΔG_0 is the free activation enthalpy of the thermal obstacles at $\sigma^* = 0$, ΔW is the mechanical activation work, k_B is the Boltzmann constant, and Δa^* is the activation area. In the case of pure materials, the activation area is related to the dislocation structure:[11]

$$\Delta a^* = \Delta x \lambda \quad [20]$$

$$\lambda = \lambda_0 \left(MGb^2/(b\sigma^* \lambda_0)\right)^{1/3} \quad [21]$$

$$\lambda_0 = \left(\frac{n_g - 1}{n_g} (\rho_{sgl} + \rho_{dip})\right)^{-0.5} \quad [22]$$

Δx is the obstacle width.

In the case of jerky motion over fixed obstacles formed by solute atoms, λ_0 depends on the solute concentration. Phenomenologically, v_g can be expressed as a unique function of effective stress.[12]

$$v_g = B \sigma^{*m} \quad [23]$$

with an exponent $m \gg 1$ and a T-dependent proportionality factor B.

b. *Viscous glide*

Alternatively, glide may be viscous in solid solutions when a cloud of foreign atoms is dragged along with the dislocations. In this case, Eq. [23] holds, too, with

$$m = 1 \quad [24]$$

$$B = B_{visc} = \frac{9 \Omega D_{sol} k_B T}{M c_0 G^2 b^7 \varepsilon_a^2 \ln(r_2/r_1)} \quad [25]$$

(Ω: atomic volume, D_{sol}: diffusion coefficient of solute atom in solvent lattice, c_0: solute concentration, $r_2 \approx \rho_{sgl}^{-0.5}$ and $r_1 \approx b$: outer and inner cut-off radius of dislocation stress field, ε_a: relative size misfit between solute and solvent atoms).[13,14] Combining the two types of obstacles, dislocations (superscript $\perp$) and solutes (superscript sol), by assuming[15]

$$\sigma^* = \sigma^{*\perp} + \sigma^{*sol} \quad [26]$$

$$v_g = v_g^{\perp} = v_g^{sol} \quad [27]$$

allows for a smooth transition from the case of pure materials, where σ^{*sol} can be neglected, to the case of strong solid-solution hardening with viscous dislocation motion, where $\sigma^{*\perp}$ is negligible.

2. *Velocity perpendicular to slip plane*

The velocity, v_c, at which dipole dislocations move perpendicularly to the slip plane is expressed in terms of climb of edge dislocations[10,14] as

$$v_c = \frac{D \Omega \sigma_c}{b k_B T} \quad [28]$$

$$\sigma_c + \frac{v_c}{B_{visc}} = \frac{Gb}{2\pi(1-\nu)} \frac{2}{d_{spon} + d_{dip}} \quad [29]$$

Table I. Parameters for Modeling

Parameter	Al	Al-5 at. % Mg	TiAl6V4
b/nm	0.286	as for Al	0.295
G	from [34]	as for Al	as for Ti[34]
ν	0.34	0.34	0.34
M	3.06	3.06	3.06
α	0.2	0.2	0.2
c_{dip}	0.2	0.2	0.2
C	1	1	1
f_{mob}	1	1	1
K_Λ	50	4	4
n_g	2	2	2
d_{spon}	6b	6b	6b
Ω	0.7 b^3	b^3	b^3
D	from [34]	1.05 D_{Al}[56,54]	0.05 D_{Ti}[56,34]
D_{sol}	—	8.0 D_{Al}[56,54]	0.045 D_{Ti}[56,34]
c_0	—	0.05	0.0418
ε_α	—	0.12 [53]	0.036[54]
$\ln(r_2/r_1)$	—	8	8
$\nu_D/^{5-1}$	10^{13}	—	—
ΔG_0/eV	1.5	—	—
Δx	b	—	—

Here, it has been assumed that edge dislocations are moving more slowly than screws and control dipole annihilation and that $\Omega \sigma_c < k_B T$. The term D is the coefficient of self diffusion. The second term on the left-hand side of Eq. [29] represents the stress for dragging a cloud of solutes; the right-hand side relates to the force by which the partners of a dipole with average spacing, $(d_{dip} + d_{spon})/2$, attract each other.

C. *Material and Model Parameters*

The model will be applied to pure Al and the alloys Al-5 at. pct Mg and TiAl6V4, where solid-solution hardening is dominant. The material and model parameters used in the constitutive equations are listed in Table I. In estimating D and D_{sol} for TiAl6V4 the Al content was neglected.

III. TRANSIENT CREEP WITH REFINEMENT OF DISLOCATION STRUCTURE

Consider a recrystallized material to be subjected to a constant stress. We assume that both the subgrain size and the initial dislocation spacing are distinctly larger than the values expected under stress. This means that the transient creep preceding the steady state, where the dislocation structure has attained the state of dynamic equilibrium, occurs under net increase in dislocation density.

A. *Pure Materials*

Figure 4 shows transients calculated from the model for pure Al. One finds normal transient (class M) behavior in that the material hardens with increasing strain (decrease of $\dot{\varepsilon}$ with ε, Figure 4(a)) and decreasing dislocation spacing (Figure 4(c)) and effective stress, σ^* (Figure 4(b)). This means that the factor v_g is dominating in Eq. [2]. The normal type of transient behavior in the primary stage of creep is generally found in pure materials and weakly hardened solid solutions of the appropriate initial state (*e.g.*, Reference 2).

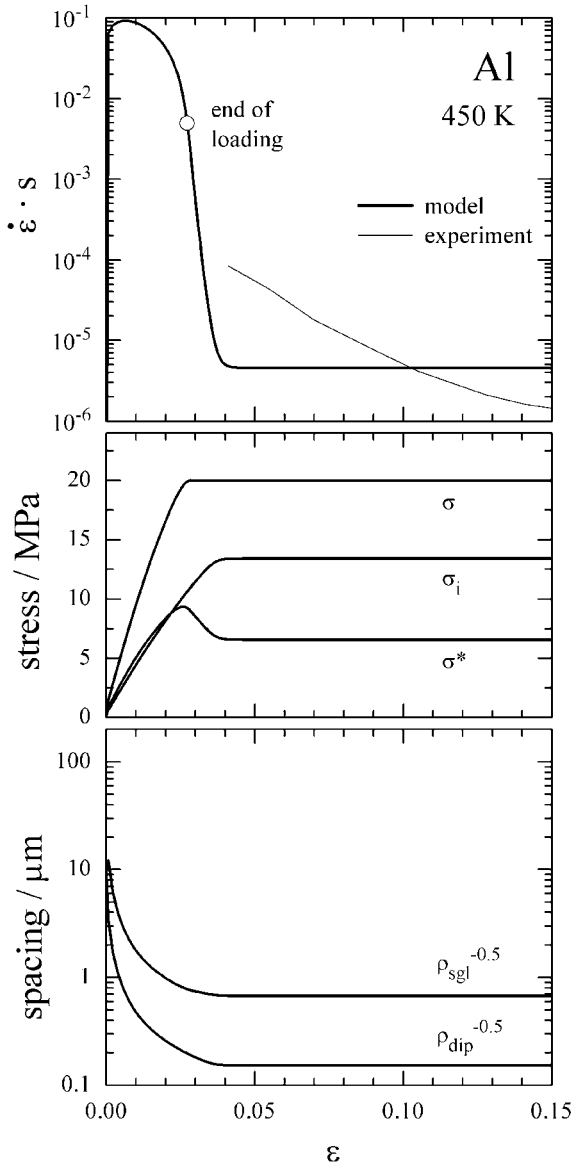

Fig. 4—Modeled transient reaction to prescribed increase of applied stress σ with time for pure Al in creep at 450 K and 20 MPa: (*a*) plastic strain rate $\dot{\varepsilon}$, with experimental curve (shifted from 523 to 450 K using an activation energy of creep of 142 kJ/mol);[55] (*b*) σ, σ^*, and σ_i; and (*c*) dislocation spacings $\rho_{sgl}^{-0.5}$ and $\rho_{dip}^{-0.5}$ as functions of plastic strain ε.

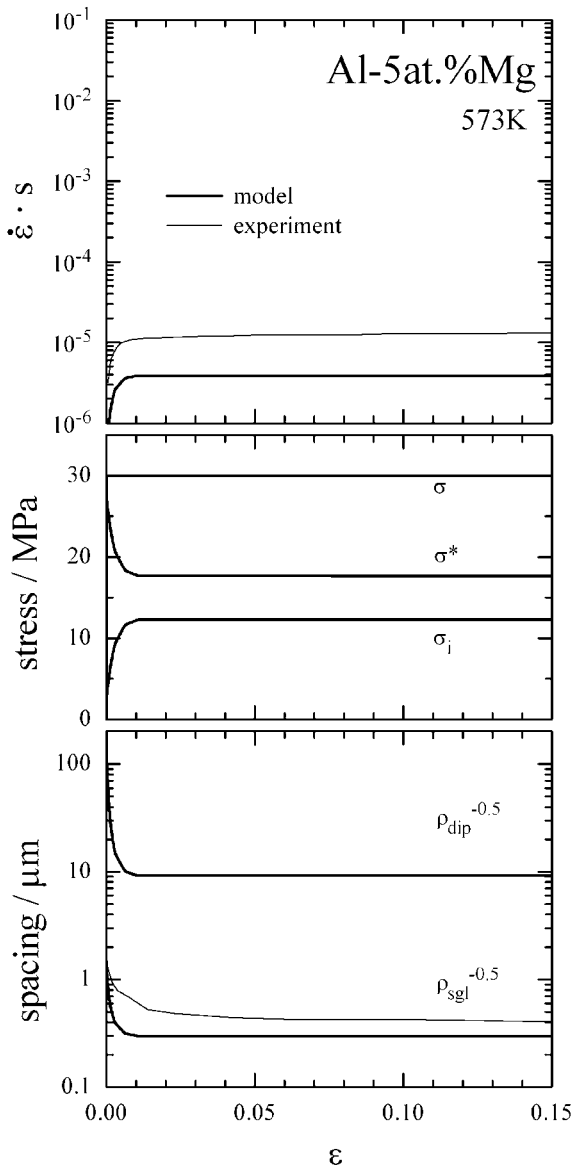

Fig. 5—Modeled transient reaction to prescribed increase of applied stress σ with time for Al-5 at. pct Mg during creep at 573 K and 30 MPa: (*a*) plastic strain rate $\dot{\varepsilon}$, with experimental curve;[27] (*b*) σ, σ^*, and σ_i; and (*c*) dislocation spacings $\rho_{sgl}^{-0.5}$ and $\rho_{dip}^{-0.5}$ as functions of plastic strain ε, with experimental data from Ref. 2.

However, the calculated transient is much shorter than the real transient as seen from comparison with the experimental curve included in Figure 4(a). During the transient, the effective stress falls to a relatively small fraction of the applied stress, which is consistent with experimental data for a weakly solution-hardened alloy.[16]

B. *Solid Solutions*

We now introduce hardening by solute drag (Eqs. [23], [24], and [25]). When the strength of solid-solution hardening is sufficiently large (small B), the character of the transient becomes inverse (class A), meaning that the material softens with increasing strain (and dislocation density) as can be seen from the experimental curve for Al-5 at. pct Mg in Figure 5(a). In contrast to the class M-case, the term ρ_{mob} in Eq. [2] is now dominating the change in $\dot{\varepsilon}$. The effective stress is a relatively large fraction of σ consistent with experiment.[17] The figure shows that the inverse transient behavior is reproduced by the model. The quantitative agreement with the measured behavior is satisfactory. Note that the ratio ρ_{sgl}/ρ_{dip} is now $\gg 1$ in contrast to the case of pure Al where it was $\ll 1$. The reason is that glide is so much slowed down by solute drag that dipoles are formed slowly and disappear relatively quickly by climb leading to a relatively low filling height of the dipole container in Figure 2.

Special effects are caused in solid solutions by changes between the two modes of dislocation motion, with and without clouds of solutes. Formation of the cloud during dynamic strain aging leads to a strong reduction in creep

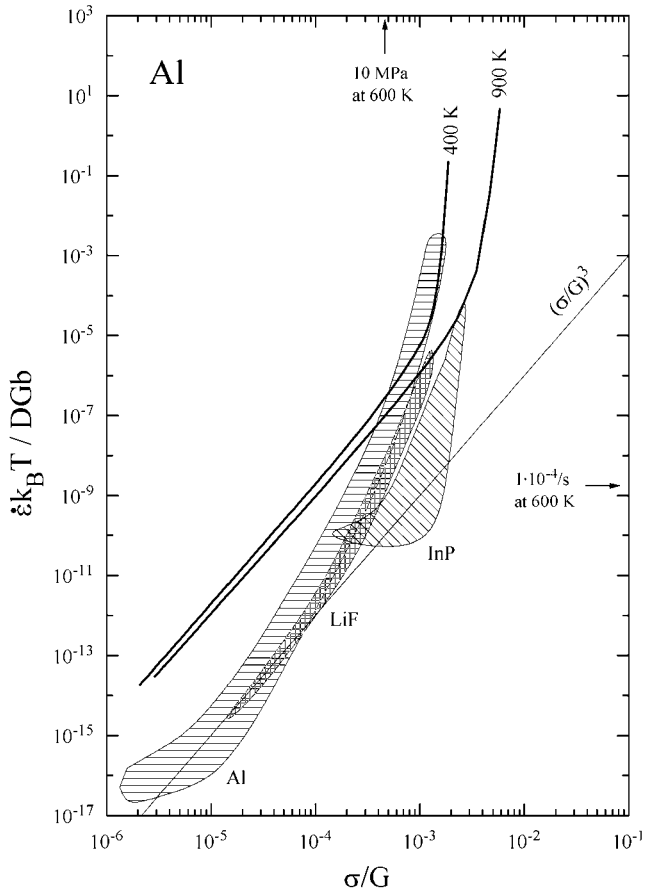

Fig. 6—Normalized steady-state strain rate–stress relation modeled for pure Al with experimental data for the pure polycrystalline fcc metal Al,[27,45], the ionic single crystal LiF,[44] and the semiconductor single crystal InP.[24]

rate followed by a relative minimum in the $\dot{\varepsilon}$-ε curve.[18,5,19] This behavior has not yet been modeled in a satisfactory manner.

IV. STEADY-STATE CREEP

A. *Pure Materials*

The steady state is reached when the dislocation structure does not change any more with strain.* Figure 6 summarizes experimental data obtained for pure materials from the group of metals, ionic crystals, and semiconductors. $\dot{\varepsilon}$ and σ are normalized. It is seen that the data approach the prediction of the natural creep law:

$$\dot{\varepsilon} = \frac{DGb}{k_B T}\left(\frac{\sigma}{G}\right)^3 \qquad [30]$$

*It is of prime importance to make sure that constancy of dislocation structure with time is not mistaken for constancy with strain. At low stress where $\dot{\varepsilon}$ is low and long times are required for small strain increments, the danger of systematic errors in determining the steady state or minimum creep rate is particularly pronounced. In the case of normal transient creep the "steady-state creep rate" will increasingly exceed the true one as the stress decreases and the strain where the "steady state" is erroneously believed to be measured decreases. This leads to a lowering of the stress exponent of the apparent steady-state creep rate with decreasing stress without a true change in creep mechanism.

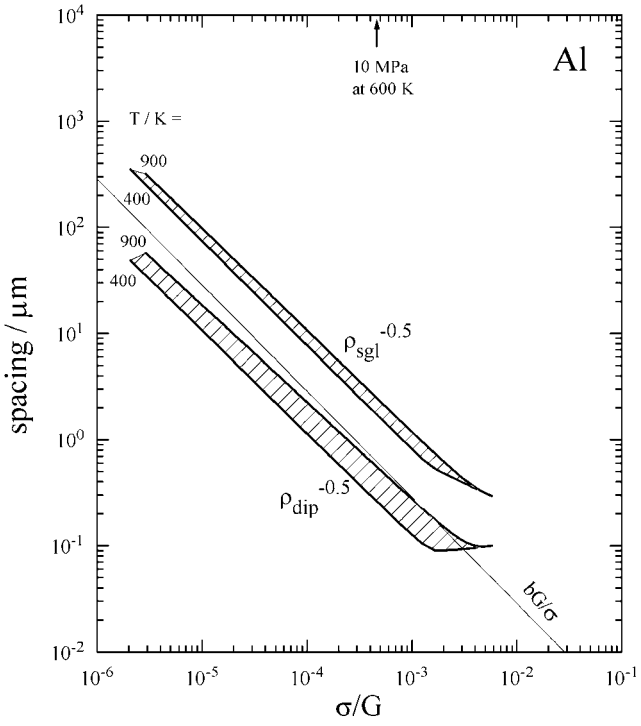

Fig. 7—Modeled steady-state dislocation spacings in pure Al as a function of shear modulus normalized stress.

with decreasing σ. This law can be derived* by assuming that a density $(\sigma/Gb)^2$ of dislocations moves at the velocity of climb, $Db^2\,\sigma/(k_BT)$.

*Within a factor M^{-1}.

A closer look shows significant variation in magnitude of the normalized creep rate. InP takes the lowest position in Figure 6. InP has a particularly low value of the stacking fault energy. Such variation with stacking fault energy is well established for metals (References 20 and 21, and further references in Reference 22). Lower stacking fault energy leads to slower climb[23] and cross slip, larger steady-state dislocation densities, and higher driving force for discontinuous dynamic recrystallization where subgrains become unstable and grow to become large grains. This happens with pure Cu, Ni, and Ag as well as with InP single crystals.[24,25]

At this point, it should be noted that it has become clear that not only the dislocation structure but also the grain structure approaches a state of dynamic equilibrium. In the absence of discontinuous dynamic recrystallization, the grains will eventually become equiaxed through geometrical dynamic recrystallization, *i.e.*, by recombination of grain boundaries, when the grains have been sufficiently thinned during monotonic deformation. We neglect dynamic recrystallization here noting that there is a discussion on whether the misorientation of subgrain boundaries naturally grows with strain so that subgrain boundaries are transformed to large angle boundaries in a process called continuous recrystallization. This term has been rejected as inappropriate by McQueen and others (Reference 26 provides details).

In addition to experimental results, Figure 6 also displays the result of calculation of the steady-state $\dot{\varepsilon}$-σ relation for pure Al with the model from Section II. The result is quite

robust against changes of parameters. In particular, strong variations of the fraction of mobile dislocations, f_{mob}, have very little influence; the reason lying in the compensating effect of the sinh term in Eq. [18]. At low stresses, the model predicts a stress exponent $n = d \log \dot{\varepsilon}/d \log \sigma$ of the steady-state creep rate in the order of 3, in agreement with the stress exponent of the natural creep law. The magnitude of the steady-state creep rate, however, is larger than predicted by the natural law. We will return to that in Section VI. In agreement with experimental results, the effect of temperature, *T*, in the three-power-law regime is relatively small with regard to steady-state creep rate and spacings of single dislocations. This is due to the fact that the activation energy chosen for thermally activated glide is quite similar to that of climb.*

*Without this choice, a distinct influence of *T* would result.

The modeled steady-state spacings of single dislocations (Figure 7) are in reasonable accordance with the spacings, $\rho_f^{-0.5}$, of free dislocations, which are observed in the subgrain interior of pure materials after cooling down under stress from creep temperature and which are mostly lying somewhat above the reference line bG/σ.[27,2,25] The average spacings of dipole dislocations are, however, distinctly smaller than $\rho_f^{-0.5}$ (Figure 7). At stresses above $10^{-3}G$, the decrease of the spacings of single dislocations slows down, and the dipole dislocation spacing starts to increase with increasing stress. The reason is that the dislocation spacings have become so small that spontaneous annihilation becomes important and finally takes over. Figure 6 shows that the steady-state creep rate increases strongly with stress above $10^{-3}G$. The three-power-law breaks down, and *n* increases to very high values.

1. *Harper–Dorn creep*

At the low stress end of the steady-state $\dot{\varepsilon}$-σ relation a special mechanism of viscous flow ($n = 1$), called Harper–Dorn creep, has first been reported for coarse-grained pure Al[28] (the lower left branch of the Al-data in Figure 6). The creep rates in this range are small, $<10^{-7}$/s, but distinctly higher than expected from diffusive flow. Blum and coworkers[27,29] criticized the weak experimental foundation of the Harper–Dorn mechanism; in particular, there exists no confirmation of $n = 1$ from stress change tests on individual specimens. The attempt to reproduce the Harper–Dorn creep results in compression tests with cubical specimens yielded lower creep rates than reported by the proponents of the Harper–Dorn mechanism, and *n*-values in the range of 6.[29]

Nabarro[30] argued that the stresses used in Reference 29 had been larger than the maximum value of 0.08 MPa where Harper–Dorn creep can be observed. Therefore, compression tests were performed at stresses from 0.06 to 0.11 MPa. While the previous measurements of creep strain reported in Reference 29 had been done in the conventional manner with extensometers transferring the positions of the upper and lower end of the compression specimen to inductive transducers, the present measurements were performed by contactless optical strain measurement with a laser beam scanning the distance between two markers on the compression specimen. Figure 8 shows the results from tests on four different rather big specimens measuring 35 mm in length with a cross section of about 29×29 mm^2. The specimens were taken from a cast bar of Al99.99. No special care was taken to unify the heat treatment, which essentially consisted of heating to test temperature and holding prior to creep for different times between 1 and 10 hours. The difference in heating may be one reason for the difference in primary creep (observed for instance between the two tests starting at 0.07 MPa), with a more pronounced transient for shorter preheating at test temperature. However, these differences should be irrelevant for the steady-state of creep. The present tests essentially confirm the previous results from compression tests.[29] The primary transient is quite pronounced in spite of the extremely low stress so that a strain of 0.01 does not guarantee steady-state conditions. Stress changes show that the stress exponent is in all cases in the range of 5, *i.e.*, far from 1. The $\dot{\varepsilon}$ data taken at the ends of the creep sections for constant stress (open symbols on the right) are plotted *vs* stress in the left part of the figure. As most of the data stem from the primary stage of creep, they are systematically high. Taking this into account, there is good agreement with the previous compression data. The compression data are well described by a straight line with slope $n = 5$.

Meanwhile McKnee *et al.*[31] have also reported that the original large $\dot{\varepsilon}$ values of the Harper–Dorn range could not be reproduced (in tensile tests with few exceptions at stresses below 0.04 MPa). Rather, the creep rate continued to decrease with continued tensile strain to extremely small values included in Figure 8. The values are somewhat lower than those from the compression tests. It must be noted here that purity has a strong influence on the creep rates at low stresses $<10^{-4}G$. Results of Straub reported in Reference 25 show that the creep rate in this stress range is decreased by several orders of magnitude by the impurities contained in Al99.5, compared to Al99.99. The differences between the compression results and the tensile results of Reference 31 are much smaller and may be explained in terms of differences in impurity content, taking into account that McKnee *et al.* used materials of different nominal purities.

Figure 9 displays the subgrains developed in the test of Figure 8 ending at a strain of 0.042 under a stress of 0.07 MPa. The steady-state subgrain size, *w*, is expected to be 1.6 mm (corresponding to $w = 23bG/\sigma$[32]). The experimental value determined for *w* from Figure 9 using the linear intercept method is 1.3 mm. This is in fair agreement with the expected steady-state value and fits to the data obtained by Barrett *et al.*[33] under Harper–Dorn creep conditions. So there is little doubt that the dislocation structure evolves in the same qualitative manner as for higher stresses, with establishment of a stress-dependent steady-state subgrain structure.

In conclusion, the compression tests clearly show that a five-power-law holds even in the range close to the melting point of Al at extremely low creep rates and that there is no change in microstructural evolution at these stresses. The measured Harper–Dorn creep rates result either from misinterpretation of primary creep rates as steady-state rates or from a microstructural difference between tensile and compression tests. Such a difference might stem from dynamic grain-boundary migration, failure by deformation instability, or specimen size. With regard to the latter, it must be kept in mind that a specimen is no longer large compared to the dislocation structural spacings at the very low stresses where the Harper–Dorn phenomenon was

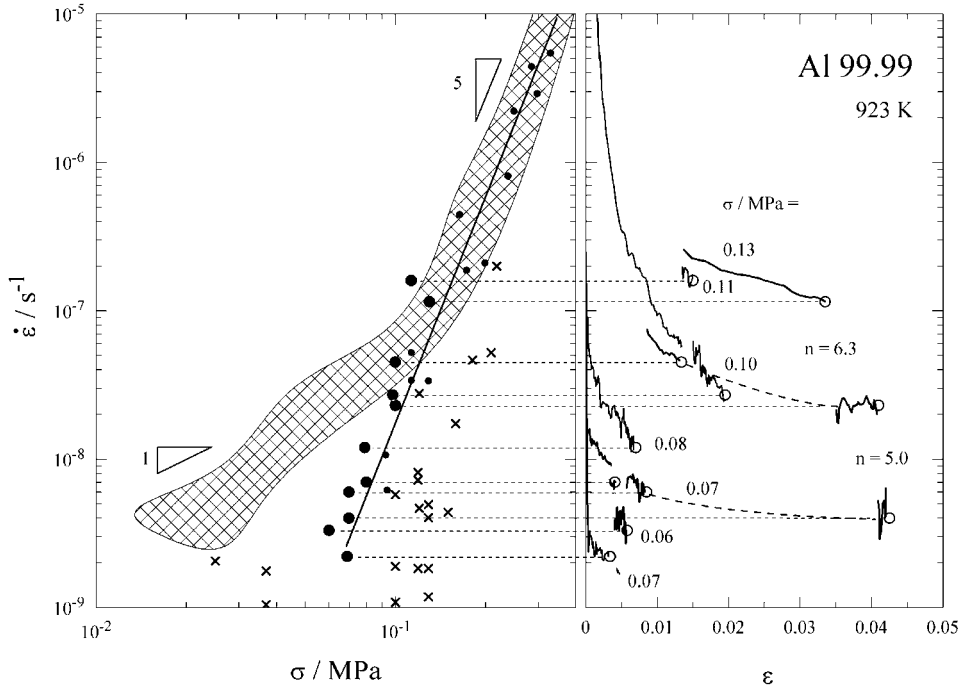

Fig. 8—Creep rate of pure Al at low stresses. Right: $\dot{\varepsilon}$-ε curves for constant compressive stress σ (relative accuracy better than 5 pct) measured with contactless laser extensometry, left: $\dot{\varepsilon}$ as function of σ, large circles: taken from the ends of test portions at constant stress, as indicated by connecting horizontal lines, small circles: from Refs. 29 and 45, crossed field: literature data as reported in Ref. 29, and crosses: from McKnee *et al.*[31]

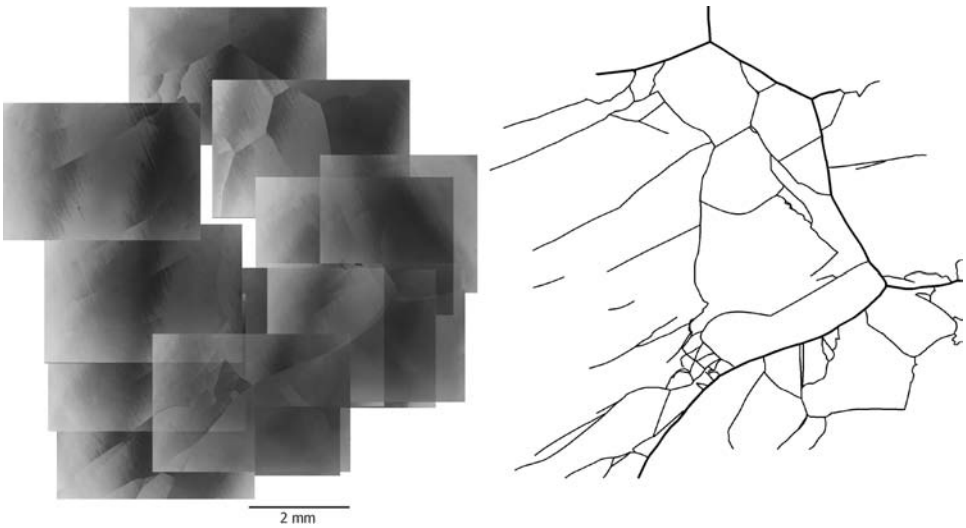

Fig. 9—Subgrain structure in Al after cooling the specimen under stress to room temperature at the end (ε = 0.042) of the longest compressive creep test shown in Fig. 8; left: montage of micrographs by SEM with backscattered electrons, and right: traces of visible subgrain boundaries (thin lines) taken from pictures with different inclinations of the electron beam to the specimen; bold lines mark large angle grain boundaries.

reported. For instance, at a stress of 0.03 MPa, one expects a subgrain size of 3.7 mm (=23bG/σ, b, and G from Reference 34) and an average spacing of dislocations inside subgrains of 0.16 mm (=bG/σ). The grains (with sizes in the cm-range[27]) and even the subgrains are so large that most of them extend up to the surface of the specimens. Grain-boundary traces at the surfaces of the compression specimens give clear evidence of long-range motion of grain boundaries. Under these circumstances, the results of compression tests with large, cm-sized, cubical specimens appear most reliable. Different results must be expected under conditions where the steady-state subgrain size approaches the specimen dimensions.[35]

2. *Diffusive flow*

The importance of diffusive flow has long been under discussion. New results prove that matter is deposited at grain boundaries by diffusive flow.[36,37] Thus, there is no doubt that diffusive flow exists. However, the observed kinetics of diffusive flow does not fully conform to the predictions of the original simple models of diffusive flow. In particular, the stress exponent of the diffusive creep rate

is generally larger than 1.[38,36,37] The reason may lie in the structure of large-angle grain boundaries. While the models assume all boundaries to act as ideal sinks and sources of vacancies, this is not the case in reality. Experimental proofs for that were given in Reference 36.

B. *Solid Solutions*

When the parameter B in Eq. [23] takes finite values, solid-solution hardening comes into play. Assuming in analogy to the derivation of the natural creep law in Section IV.A that a density $(\sigma/Gb)^2$ of dislocations moves viscously at the velocity given by Eqs. [23], [24], and [25] with $\sigma^* = \sigma$, one obtains for the steady-state kinetics of solid solutions:

$$\dot{\varepsilon} = A\frac{DGb}{k_B T}\left(\frac{\sigma}{G}\right)^3 \quad A = \frac{9}{M^2 c_0 \varepsilon_a^2 \ln(r_2/r_1)}\frac{D_{sol}}{D}\left(\frac{k_B T}{Gb^3}\right)^2 \qquad [31]$$

which differs from the natural law Eq. [30] for pure materials only by the numerical factor, A, depending on alloy characteristics and T.

A particularly strong effect is found for the alloy TiAl6V4. The experimental data show a marked change in the steepness of the normalized $\dot{\varepsilon}$-σ relation in Figure 10 at $\sigma \approx 2 \cdot 10^{-2}G$. At lower stresses, the experimental data are in approximate agreement with Eq. [31]. Model curves were calculated on the basis of viscous glide; these provide a good description of the experimental results for stresses up to $10^{-2}G$. For $\sigma > 2 \cdot 10^{-2}G$, however, the viscous law fails and one needs Eq. [23] with $m = 30$ to model the experimental results in terms of thermally activated jerky glide over fixed solute obstacles.

The steady-state spacings of single dislocations (Figure 11) are of the expected order of magnitude somewhat above bG/σ. In contrast to the model results for pure Al, the average spacing of dipole dislocations is much larger than that of single ones. This means that the dipoles have enough time to climb away during viscous glide. The picture changes above $10^{-2}G$ where spontaneous annihilation must no longer be neglected. The density of single dislocations saturates, and the density of dipoles decreases strongly with increasing stress as the spontaneous annihilation of single dislocations is sufficient to carry all the dislocation annihilation.

According to this interpretation, steady-state deformation must be completely glide-controlled beyond the viscous range. This is in fact supported by the observation of a range with negative $\dot{\varepsilon}$ dependence of the steady-state flow stress in the transition between the viscous and the jerky ranges,[39] which finds a natural explanation in terms of glide being influenced by dynamic strain aging.*

*That is, thinning of the cloud of solutes as the dislocation velocity is increased; not incorporated in the present model.

TiAl6V4 represents an extreme case of solid-solution hardening at relatively low homologous temperature of about 0.3. In other cases, the transition from viscous to jerky dislocation motion of dislocations during steady-state creep occurs at smaller stresses and, therefore, is less pronounced. For instance in Al-2.2 at. pct Mg the transition was reported to occur at $\sigma = 1.4 \cdot 10^{-3}G$, and the stress exponent increases by a limited amount from 3 to 5.[40,41] Weakly solid-solution hardened alloys, such as Al-5 at. pct Zn, even behave similar to pure metals (class M) with little influence of solid-solution

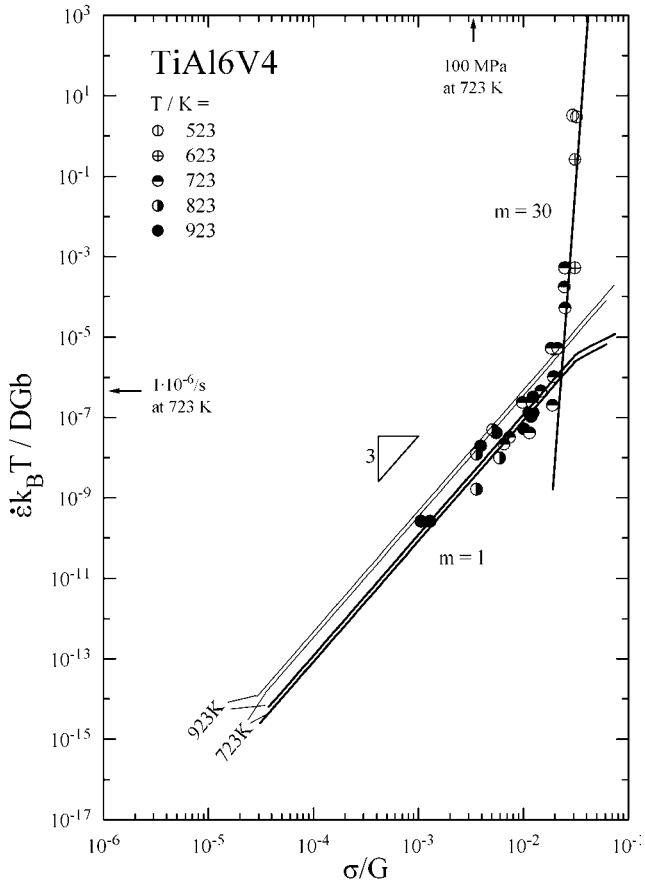

Fig. 10—Normalized steady-state strain rate–stress relation for TiAl6V4. Experimental data from Ref. 39. Thin lines: Eq. [31], and bold lines from model with Eq. [23] for viscous glide (Eqs. [24] and [25]) and jerky glide with $m = 30$.

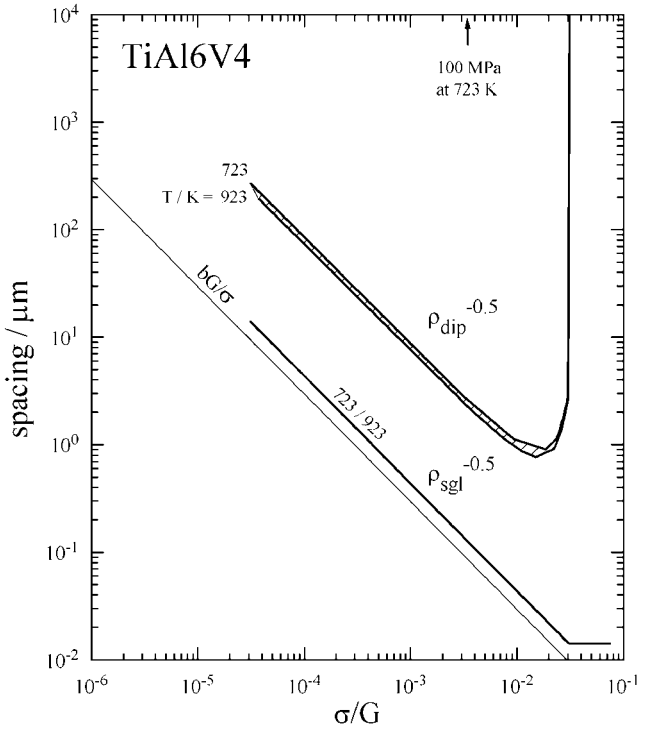

Fig. 11—Modeled steady-state dislocation spacings in TiAl6V4 as a function of shear modulus normalized stress.

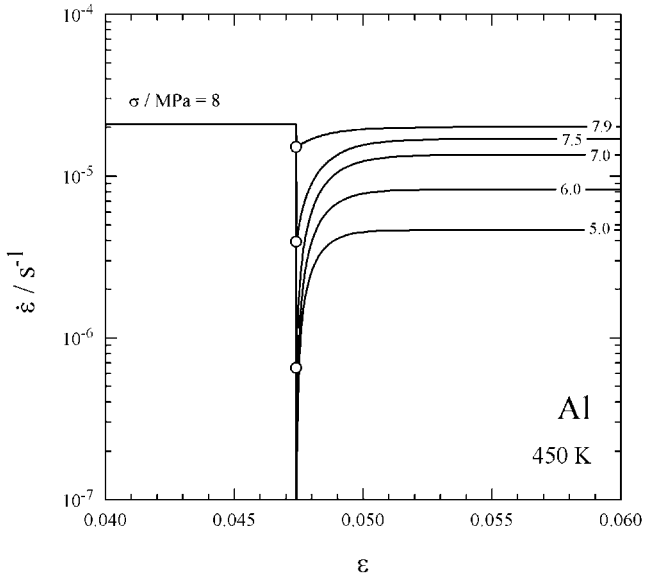

Fig. 12—Modeled transient creep after sudden stress reductions during steady-state creep of pure Al.

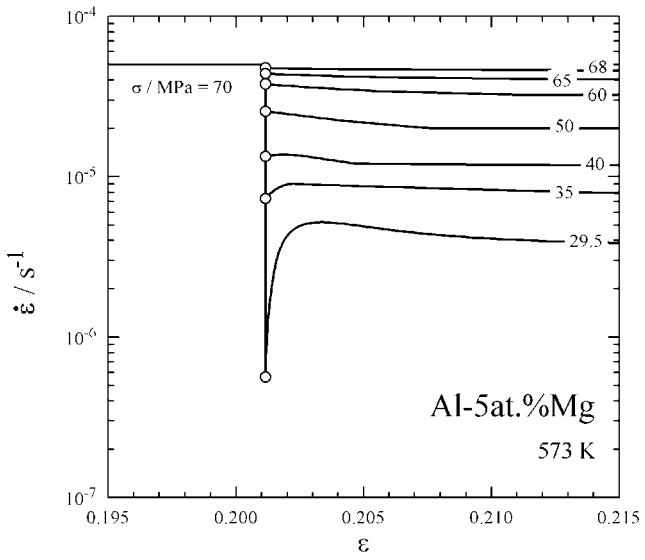

Fig. 13—Modeled transient creep after sudden stress reductions during steady-state creep of Al-5 at. pct Mg.

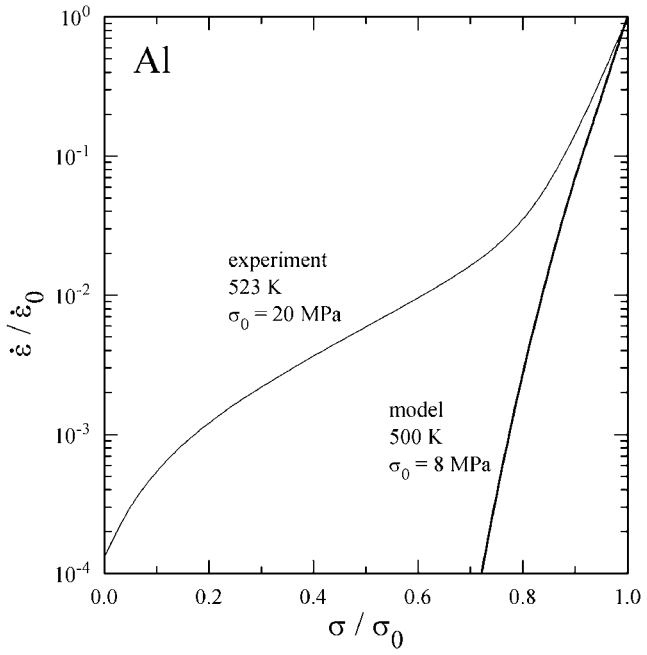

Fig. 14—Thin lines: positive creep rate at the beginning of the transients after stress reduction during steady-state creep of Al at rate $\dot{\varepsilon}_0$ and stress σ_0 as a function of reduced stress σ from Ref. 2, and bold lines: modeled initial transient creep rates.

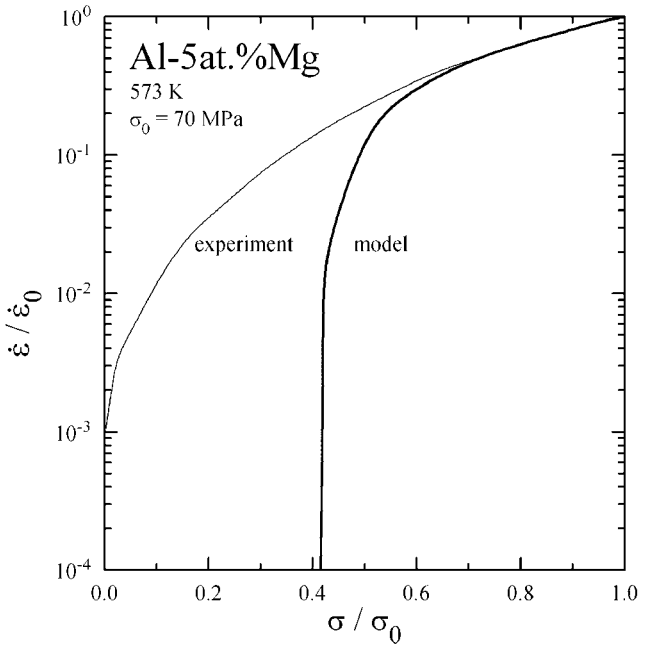

Fig. 15—Thin lines: positive creep rate at the beginning of the transients after stress reduction during steady-state creep of Al-5 at. pct Mg at the rate $\dot{\varepsilon}_0$ and the stress σ_0 as a function of reduced stress σ from Ref. 2, and bold lines: modeled initial transient creep rates.

hardening on the steady state (but distinct reduction of the $\dot{\varepsilon}$ variation during transient creep).[2]

V. TRANSIENT CREEP WITH NET COARSENING OF DISLOCATION STRUCTURE

After a sudden reduction in stress, the dislocation structure coarsens. The accompanying transient reaction differs for materials of classes M and A, being normal and inverse, respectively, for relatively small stress reductions.[2]

Figure 12 and 13 display the modeled behavior for selected stress reductions. As the model in its present form is only able to handle positive effective stresses, the maximum stress reductions are limited. It is seen that the normal and inverse transients are well reproduced for small stress reductions. For large stress reduction, however, there is a qualitative discrepancy between the modeled (normal) and the measured (inverse) transient behavior of Al-Mg. In reality, the transient response *after* relatively large, sudden reductions in stress (and the accompanying sudden drops in $\dot{\varepsilon}$) is characterized by a pronounced initial decrease in $\dot{\varepsilon}$ with ε, before the normal or inverse transient behavior is resumed.[2]

Figures 14 and 15 show the positive creep rate measured just after the elastic reaction and, if appropriate, the anelastic back flow. It is seen that the modeled data are in good accord with the experimental data for small relative reductions in σ. For larger reductions, however, the model fails for pure Al as well as for the alloy, the observed creep rates being much larger than the modeled ones.

We mention in passing that special transient effects are observed in the case of dynamic strain aging. There is an initial increase/decrease in $\dot{\varepsilon}$ immediately after an increase/decrease in σ as the cloud of solute atoms thins/builds up.[18,19] These transients are superimposed on the transient reactions resulting from the changes of the dislocation structure and are not further treated here.

VI. DISCUSSION

Despite its simplicity in comparison to the more elaborate models of Nes[6] and Roters *et al.*,[8] the present model yields some basic understanding of creep phenomena. With the introduction of the density of dipoles as evolving microstructural parameter, it is possible to calculate the evolution of the dislocation structure from constitutive laws on a clear microstructural basis, free from restriction by phenomenology. The model reproduces important features of creep, namely, the normal and inverse transient reactions during primary creep, the power law for steady-state deformation, and its breakdown at high stresses for pure materials and alloys. The traditional distinction between *recovery-* or *climb-controlled creep* in class M (pure metals and weakly solute hardened) alloys and *glide-controlled creep* in class A (strongly solute hardened) alloys has been confirmed. The calculated densities of single dislocations lie in a reasonable range; this is achieved by the condition $\sigma^* > 0$ for $\sigma > 0$, putting a limit on the dislocation densities according to Eqs. [16] and [17].

An important new feature of the model is the distinction between low temperature deformation at high stress, where dynamic recovery occurs as a byproduct of glide *via* spontaneous annihilation of dislocations, and high temperature deformation at low stress, where it needs diffusion-controlled climb to attain the steady state. The present modeling gives support to the qualitative interpretation of the power-law breakdown in terms of spontaneous annihilation proposed by Reference 42. Corresponding to the different levels of sophistication, there are quantitative differences. The estimate in Reference 42 resulted in an infinite slope beyond the power-law breakdown; the present, more detailed one shows that the slope of the normalized curve in Figure 6 is finite, being determined by the stress dependence of the rate of thermally activated glide at the modeled dislocation structure.

While the simple model works without problems for the solute hardened alloy, there are deficits regarding the quantitative agreement with experiment for pure materials as

(1) the creep transients are too short,
(2) the density of dipoles is too high compared to experimental evidence,
(3) the steady-state creep rate is too large (steady-state flow stress too small) in the range with constant power $n = 3$, and
(4) the power-law breakdown is too sharp so that an extended region with an average stress exponent 5 of the steady-state creep rate is missing.

Anelastic reactions have not been included in the model so far. This is not really a deficit of the model, but results from the simplification to set the parameter C in Eq. [17] equal to 1.

The quantitative deficiency of the model, in the case of pure materials, can be linked to the density of stored dipoles. In the high temperature case, where spontaneous annihilation is negligible, it is evident from Figure 2 that $\dot{\rho}^+_{\text{sgl}}$ must equal $\dot{\rho}^-_{\text{dip,c}}$ under steady-state conditions where inward and outward flows of dislocations compensate each other. It follows from Eqs. [8], [9], and [12] that the steady-state rate is

$$\dot{\varepsilon} = \frac{b}{M}\, k_\Lambda\, \rho^{-0.5}\, \rho_{\text{dip}}\, \frac{4v_c}{d_{\text{dip}}}. \qquad [32]$$

As v_c and d_{dip} are unique functions of applied stress at a given T (Eqs. [13], [28], and [29]), and k_Λ varies only by a limited amount (Table I), the modeled large difference between pure and solute hardened materials must stem from the steady-state dislocation densities. In fact, comparison of Figures 7 and 11 shows that there is a difference in the steady-state ρ_{dip} by a factor of $>10^3$. This suggests that the model allows the pure material to store an unrealistically large number of dipoles.

If the modeled curve in Figure 6 would be shifted downward by an appropriate modeling measure to fit the experimental data in Figure 6 at low stresses $\approx 10^{-4}G$, the problem would remain that the modeled stress exponent 3 is smaller than the exponent 5, which is generally considered characteristic of the power-law range in pure materials for "*climb-controlled creep*" (refer to the recent review[43]). Two comments shall be made here. First, $n = 5$ is not always observed. In fact, "natural" behavior with $n = 3$ has been found in pure LiF single crystals at low stresses below $10^{-4}G$ (Figure 7) and has been confirmed by stress change tests on individual specimens.[44] The artificially grown LiF single crystals were of extraordinary purity. In Al, a clear effect of purity has been established, with n increasing strongly with impurity at $\sigma < 10^{-4}G$.[25] Thus, the deviation of the experimental data from the three-power-law may be an impurity effect influencing the data for pure Al below $\sigma = 10^{-4}G$.[45] Second, Nes *et al.*[6,46,35] have offered three arguments for n being larger than 3. One is a factor, bc_j, entering the formula for the climb velocity (Eq. [28]), with c_j being the density of jogs along the climbing edge dislocations. This factor is < 1 and $\propto \rho^{0.5}$; it raises n from 3 to 4. Another argument is the limitation of Λ^+ by grain boundaries at small stresses, bringing n up from 4 to >5. Without further discussion, we state that these arguments are in principle good for reducing the steady-state creep rate at small stresses. The third proposal of Nes *et al.* is that annihilation of edge dislocation dipoles is speeded up by the fast climb of the rounded ends of the dissolving edge dipoles. This may well be a valid argument for relatively large stresses $\sigma > 10^{-4}G$ where the smooth deviation from the power law sets in before spontaneous annihilation takes over. However, the criticism[47] remains that the mediating action of subgrain boundaries has not been taken into account by Nes *et al.*

The heterogeneity of the dislocation structure in the form of subgrains has been neglected also in the present simple model. The subgrains stem from a patterning process leading to the grouping of dislocations into a dislocation-poor cell interior and dislocation-rich cell boundaries.[48,49] As the cell boundaries carry distinct misorientations after deformation

at high temperatures, they are generally addressed as subgrain boundaries, even though the continuous passage of free dislocations creates considerable disorder at the boundaries during deformation. The necessity of passage of subgrain boundaries follows from the maximum radius, r, of dislocation loops. For pure Al, $r = 2\ \Lambda^+$ (Section II–A–1) equals $100\rho^{-0.5}$ according to Table I, which, in turn, is about 50 bG/σ according to Figure 7. The experimentally observed steady-state subgrain size is $w \approx 23\ bG/\sigma$.[32,2] Thus, $r > w$; in other words, single dislocations must pass subgrain boundaries. This reduces the average velocity of glide. The composite model accounts for this deceleration by enforcing the buildup of internal back stresses.[50,51]*

*Experimental results on the primary transient creep of the weakly solid-solution hardened (class M) alloy Al-Zn clearly support this picture. While the density of dislocations in the subgrain interior is quickly established in agreement with the present model, the building of the subgrain structure continues over much larger strains and is accompanied by significant reduction of the creep rate towards the steady state.[27]

It is suggested that the modification of the model by subgrain formation has important consequences for class M materials and may bring the model into agreement with reality. The transients get longer, the steady-state creep rate in the power-law range is reduced due to back stresses of some kind, and dipole formation and dissolution are significantly modified by the two-dimensional dislocation network of the subgrain boundaries.

A point, where the present model fails even qualitatively both for pure and solute hardened materials, is the transient behavior after stress reductions (Section V). Such stress reductions occur frequently in practice, *e.g.*, after unloading events or during stress relaxation. The relatively high values of creep rate after stress reduction have been explained in terms of strain associated with recovery.[5] Subgrain boundary migration is one process where strain is created during recovery (as the subgrains coarsen). Experimental observations on subgrain boundary migration in LiF could quantitatively explain the observed effect.[52] Thus, subgrain boundaries appear to be of importance here, too.

VII. SUMMARY

Experimental results on the kinetics of creep and the microstructural evolution have been compared with the predictions of a simple spatially homogeneous model of plastic deformation. The merging of slipped areas by formation and disappearance of dislocation dipoles has been explicitly incorporated in the model. The model yields the evolution of the dislocation structure as well as the kinetics of creep. It gives basic insight into creep phenomena like transient and steady-state creep, power laws of steady-state creep and their breakdown at high stresses, and the strong influence of solutes. Particular attention has been paid to the points where the model fails. The inability to predict the low stress-low creep-rate phenomenon of viscous Harper–Dorn creep is not considered a failure of the model, as Harper–Dorn creep is absent in uniaxial compression of large cubical specimens of Al, indicating that it lacks the generality ascribed to it in the literature. The main reasons for observed deficiencies of the model are supposed to lie in the neglection of dislocation patterning (subgrain formation) and of the strain associated with recovery.

ACKNOWLEDGMENTS

Financial support by the Bayerische Forschungsstiftung and Audi AG, Bundesministerium für Bildung und Forschung and Schott Lithotec AG, and the Deutsche Forschungsgemeinschaft is gratefully acknowledged. Thanks are due to Professor E. Nes for valuable discussions.

REFERENCES

1. H. Alexander and P. Haasen: *Solid State Phys.*, 1968, vol. 22, p. 27.
2. W. Blum: in *Plastic Deformation and Fracture of Materials*, H. Mughrabi, ed., vol. 6 *Materials Science and Technology*, R.W. Cahn, P. Haasen, and E.J. Kramer, eds., VCH Verlagsgesellschaft, Weinheim, 1993, pp. 359-405.
3. J. Weertman: *Trans. AIME*, 1960, vol. 218, pp. 207-18.
4. J. Weertman: *Trans. ASM*, 1968, vol. 61, pp. 681-94.
5. W. Blum: *Mater. Sci. Eng. A*, in press.
6. E. Nes: *Progr. Mater. Sci.*, 1998, vol. 41, pp. 129-93.
7. F. Roters: Berichte aus der Werkstofftechnik, D 82 (Diss. RWTH Aachen), Shaker Verlag, Aachen, 1999.
8. F. Roters, D. Raabe, and G. Gottstein: *Acta Mater.*, 2000, vol. 48, pp. 4181-89.
9. U. Essmann and H. Mughrabi: *Phil. Mag.*, 1979, vol. 40, pp. 731-56.
10. Peter Haasen: *Physikalische Metallkunde*. Springer-Verlag, Berlin, 1974.
11. H. Kronmüller: *Moderne Probleme der Metallphysik*, Springer, Berlin, 1965, vol. 1, pp. 126-91.
12. U.F. Kocks: *J. Eng. Mater. Technol. (ASME-H)*, 1976, vol. 98, pp. 76-85.
13. A.H. Cottrell and M.A. Jaswon: *Proc. R. Soc.*, 1949, vol. A199, p. 104.
14. S. Takeuchi and A.S. Argon: *Acta Metall.*, 1976, vol. 24, pp. 883-89.
15. Q. Zhu and W. Blum: *Proc. 7th JIM Int. Symp. on Aspects of High Temperature Deformation and Fracture in Crystalline Materials*, Y. Hosoi, H. Yoshinaga, H. Oikawa, and K. Maruyama, eds., The Japan Institute of Metals, Sendai, 1993, pp. 649-56.
16. W. Blum and A. Finkel: *Acta Metall.*, 1982, vol. 30, pp. 1705-15.
17. W. Blum and E. Weckert: *Mater. Sci. Eng.*, 1987, vol. 23, pp. 145-58.
18. S.U. An, H. Wolf, S. Vogler, and W. Blum: in *Creep and Fracture of Engineering Materials and Structures*, B. Wilshire and R.W. Evans, eds., The Institute of Metals, London, 1990, pp. 81-95.
19. F. Breutinger and W. Blum: *Proc. 9th Int. Conf. on Creep and Fracture of Engineering Materials and Structures*, J.D. Parker, ed., The Institute of Metals, London, 2001, pp. 39-48.
20. C.R. Barrett and O.D. Sherby: *Trans. AIME*, 1965, vol. 233, p. 1116.
21. H. Mecking, B. Nicklas, B. Zarubova, and U.F. Kocks: *Acta Metall.*, 1986, vol. 34, pp. 527-35.
22. J. Čadek: *Creep in Metallic Materials*, Elsevier, Amsterdam, 1988.
23. A.S. Argon and W.C. Moffatt: *Acta Metall.*, 1981, vol. 29, pp. 293-99.
24. B. Geibel: Ph.D. thesis, University of Erlangen-Nürnberg, Erlangen, 1996.
25. W. Blum: *The Johannes Weertman Symp.*, R.W. Arsenault, D. Cole, T. Gross, G. Kostorz, P. Liaw, S. Parameswaran, and H. Sizek, eds., TMS, Warrendale, PA, 1996, pp. 103-17.
26. H. McQueen: *Metall. Mater. Trans. A*, 2002, vol. 33A, pp. 345-62.
27. W. Blum: *Hot Deformation of Aluminum Alloys*, T.G. Langdon, H.D. Merchant, J.G. Morris, and M.A. Zaidi, eds., TMS, Warrendale, PA, 1991, pp. 181-209.
28. J. Harper and J.E. Dorn: *Acta Metall.*, 1957, vol. 5, p. 654.
29. W. Blum and W. Maier: *Phys. Status Solidi (a)*, 1999, vol. 171, pp. 467-74.
30. F.R.N. Nabarro: *Phys. Status Solidi (a)*, 2000, vol. 182, pp. 627-29.
31. K.R. McKnee, H.K.R. Jones, and G.W. Greenwood: *Proc. 9th Int. Conf. on Creep and Fracture of Engineering Materials and Structures*, J.D. Parker, ed., The Institute of Metals, London, 2001, pp. 185-95.
32. S.V. Raj and G. Pharr: *Mater. Sci. Eng.*, 1986, vol. 81, pp. 217-37.
33. C.R. Barrett, E.C. Muehleisen, and W.D. Nix: *Mater. Sci. Eng.*, 1972, vol. 10, pp. 33-42.
34. H.J. Frost and M.F. Ashby: *Deformation-Mechanism Maps*, Pergamon Press, Oxford, United Kingdom, 1982.
35. E. Nes, W. Blum, and P. Eisenlohr: *Metall. Mater. Trans. A*, 2002, vol. 33A, pp. 305-10.
36. P.A. Thorsen and J. Bilde-Sørensen: *Mater. Sci. Eng. A*, 1999, vol. 265, pp. 140-45.

37. K.R. McKnee, H.K.R. Jones, and G.W. Greenwood: *Proc. 9th Int. Conf. on Creep and Fracture of Engineering Materials and Structures*, J.D. Parker, ed., The Institute of Metals, London, 2001, pp. 3-13.
38. A. Rendtel, H. Hübner, M. Herrmann, and C. Schubert: *J. Am. Ceram. Soc.*, 1998, vol. 81(5): pp. 1109-20.
39. F. Hebner: Master's Thesis, Universität Erlangen-Nürnberg, Erlangen, 2000.
40. H. Oikawa, K. Sugawara, and S. Karashima: *Scripta Metall.*, 1976, p. 885.
41. H. Oikawa and T.G. Langdon: in *Creep Behaviour of Crystalline Solids*, B. Wilshire and R.W. Evans, eds., Pineridge Press, Swansea, 1985, pp. 33-82.
42. W. Blum and F. Roters: *Phys. Status Solidi (a)*, 2001, vol. 184, pp. 257-61.
43. M.E. Kassner and M.-T. Pérez-Prado: *Progr. Mater. Sci.*, 2000, vol. 45(1), pp. 1-102.
44. M. Biberger and W. Blum: *Scripta Metall.*, 1989, vol. 23, pp. 1419-24.
45. S. Straub and W. Blum: *Scripta Metall. Mater.*, 1990, vol. 24, pp. 1837-42.
46. E. Nes, T. Pettersen, and K. Marthinsen: *Scripta Mater.*, 2000, vol. 43, pp. 55-62.
47. W. Blum: in *Light Metals 99*, M. Bouchard and A. Faucher, eds., Canadian Institute of Mining, Metallurgy and Petroleum, Montreal, 1999, pp. 521-36.
48. R. Sedláček, J. Kratochvíl, and W. Blum: *Phys. Status Solidi (a)*, 2001, vol. 186, pp. 1-16.
49. R. Sedláček, W. Blum, J. Kratochvíl, and S. Forest: *Metall. Mater. Trans. A*, 2002, vol. 33A, pp. 319-27.
50. S. Vogler and W. Blum: *Creep and Fracture of Engineering Materials and Structures*, B. Wilshire and R.W. Evans, eds., The Institute of Metals, London, 1990, pp. 65-70.
51. R. Sedláček, S. Straub, A. Borbély, T. Ungár, and W. Blum: *Plasticity of Metals and Alloys (ISPMA 6)*, P. Lukáč, ed., vols. 97–98, *Key Engineering Materials*, E. Armanios, Y.-W. Mai, and F.H. Wöhlbier, eds., Trans Tech Publications, Aedermannsdorf, Switzerland, 1994, pp. 461-66.
52. W. Müller, M. Biberger, and W. Blum: *Phil. Mag. A*, 1992, vol. 66, pp. 717-28.
53. P. Yavari, F.A. Mohamed, and T.G. Langdon: *Acta Metall.*, 1981, vol. 29, pp. 1495-1507.
54. *Smithells Metals Reference Book*, 7th ed., E.A. Brandes and G.B. Brook, eds., Hartnolk Ltd., Bodmin, Cornwall, 1992.
55. T. Pöllmann: Ph.D. Thesis, Universität Erlangen-Nürnberg, Erlangen, 1994.
56. K. Linga Murty, F.A. Mohamed, and J.E. Dorn: *Acta Metall.*, 1972, vol. 20, pp. 1009-18.